Influence of Interfacial Dynamics and Multi-Dimensional Coupling from Isolator Brackets on Exhaust Isolation System Performance

UNDERGRADUATE HONORS THESIS

Presented in Partial Fulfillment of the Requirements for Graduation with Honors Research Distinction in the Department of Mechanical and Aerospace Engineering at The Ohio State University

By

Joel Taylor Bruns

Undergraduate Program in Mechanical Engineering

The Ohio State University

2016

Honors Thesis Committee:

Dr. Jason Dreyer, Advisor

Dr. Rebecca Dupaix

Abstract

An automotive exhaust structure is a primary structure-borne noise path by which vibratory forces from the powertrain are transmitted to the vehicle body. The exhaust structure is typically connected to the vehicle body through a system of brackets containing elastomeric isolators, serving as the principal means of vibration isolation. In exhaust isolator system design, the isolator brackets are often modeled as simple springs. This approach neglects the effects of interfacial dynamics and multi-dimensional coupling, which result from distributed mass and stiffness throughout the isolator brackets. Accordingly, the objective of this research is to better understand how the interfacial dynamics and multi-dimensional coupling of the isolator brackets affect the exhaust isolation system performance in the 0-100 Hz range. Therefore, models with a proper representation of these interfacial dynamics and multi-dimensional coupling are created using finite element analysis (FEA) and then parameterized into multi-dimensional lumped parameter models through correlation of static and modal testing on the components and assembled system. The dynamic responses from the models for the exhaust structure and isolator brackets are then combined into a system-level model through a frequency-response-function-based substructuring method. A design study is conducted on the system-level model by systematically changing component parameters and evaluating the effect on the transmitted vertical body forces. The results show that the inclusion of these interfacial dynamics have nominal influence on isolation performance; however, the coupling terms show an observable influence, typically

increasing the force transmitted to the vehicle body. In addition, the study identified additional design modifications that could improve isolation performance, such as an increase in isolator material loss factor and an increase in the isolator fore-aft stiffness. Although the results are specific to this isolation system design, the modeling procedure outlined has the potential to be used early in the vehicle design process to identify improvements to other baseline designs.

Acknowledgements

I would like to acknowledge the National Science Foundation Industry/University Cooperative Research Centers (NSF I/UCRC) program for supporting this work. In addition, I would like to thank the industrial sponsors of this work within the NSF I/UCRC Smart Vehicle Concepts Center and Tenneco, Inc., in particular Hal Henry and Guy Smith. Finally, I would like to express my gratitude to Prof. Rajendra Singh, Prof. Jason Dreyer, Dr. Scott Noll, and the members of the Acoustics and Dynamics Laboratory at The Ohio State University for having helped me immeasurably over the years and for having opened up this invaluable opportunity for me.

Vita

March 29, 1994	Born – Fort Wayne, Indiana
June 2012	Adena High School, Frankfort, Ohio
May 2014 – Present	Undergraduate Research Assistant, Department of Mechanical and Aerospace Engineering, The Ohio State University

Fields of Study

Major Field: Mechanical Engineering

Main Focus Areas: Structural Dynamics, Finite Element Analysis, Experimental Methods

Table of Contents

List of Figures

List of Tables

1 Introduction

1.1 Exhaust Isolation and Influence on Cabin Noise

In automotive applications, the exhaust structure is a primary structure-borne noise path by which vibratory forces from the powertrain are transmitted to the vehicle body. The effects of these forces can be observed in the vehicle cabin as both vibration and acoustic noise. The exhaust structure is connected to the vehicle body through a system of brackets and elastomeric mount isolators. These isolator brackets are the principal means by which the powertrain vibratory forces that are transferred through the exhaust structure can be isolated from the vehicle body.

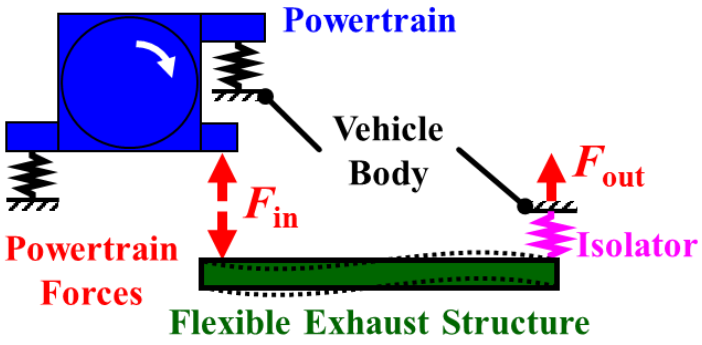

Figure 1: Powertrain Vertical Forces

Typical practice in exhaust isolation design includes the identification of exhaust hanger locations and isolator stiffness based on the modal response of an exhaust structure [1]. The effects of such isolator dynamics within a vehicle system are often evaluated through a frequency-domain synthesis method, where the dynamic responses of the components within the system are mathematically combined to evaluate a system response [2]. In these studies, within the critical 0 to 100 Hz frequency range where the cabin noise is most sensitive to forces at the exhaust connections [3], the isolator brackets

are often modeled as simple springs. This approach neglects the interfacial dynamics and multi-dimensional coupling of the isolator bracket, and with this simplification, also neglects the complex interaction with the exhaust structure which critically affects the isolation of forces transferred into the vehicle body [3]. Therefore, for proper exhaust isolation system design, these interfacial dynamics and multi-dimensional coupling must be incorporated into the system-level models.

1.2 New Obstacles for Vibration Isolation

Demand for improved fuel economy and performance in automobiles is driving vehicle structures to become lighter. These lighter structures often tend to be more sensitive to existing dynamic excitations and, as consequence, new noise and vibration problems are exposed. In addition, with the lighter vehicle structures the typical isolation regime is shifted, making traditional isolator design more difficult.

Another challenge for isolation design is that in order to improve fuel economy and vehicle performance, the automobile industry has seen a growing emergence and popularity of different powertrain technologies implemented; however, these new technologies often introduce additional noise and vibration sources into the vehicle systems. One example of a new powertrain technology is the appearance of selective cylinder management. Because this technology relies on disabling two or more cylinders under low load, the engine dynamics can change drastically, posing a challenge for vibration isolation. Another potential change in dynamic excitation is that from forced induction engines, utilizing either turbochargers or superchargers. Under load, this application could induce considerably higher vibration inputs from the powertrain. An additional consideration is hybrid powertrains, in which the engine may be routinely shut

off and started again. This can lead to harsh vibrations on engine start up as well as times of no vibration participation from the engine while shut off.

These obstacles, along with the interest in reducing design cycle time and prototyping, drive the need for system-level models with appropriate fidelity at the interfaces between systems to be developed in order to anticipate and address these new potential noise and vibration problems early in the design phase.

1.3 Interfacial Dynamics

In system level analysis, individual components are often simplified to reduce model size and complexity. In exhaust isolation design, components such as the exhaust isolator bracket assembly are often simplified as stiffness elements; consequently, certain dynamics are not accounted for in the system response. Because the isolator bracket has an associated mass, simplifying it to a stiffness element neglects additional degrees of freedom (DOF) present. Accounting for this component mass in the response is the inclusion of interfacial dynamics. This effect is illustrated in Figure 2 using a simplified model with one-dimensional springs, one-dimensional masses, and frequency responses in magnitude. From this simple example, the importance of interfacial dynamics can be illustrated. Depending on the contribution of the components at the system level, the absence of interfacial dynamics in these components can lead to an inaccurate system response, making isolation design ineffective.

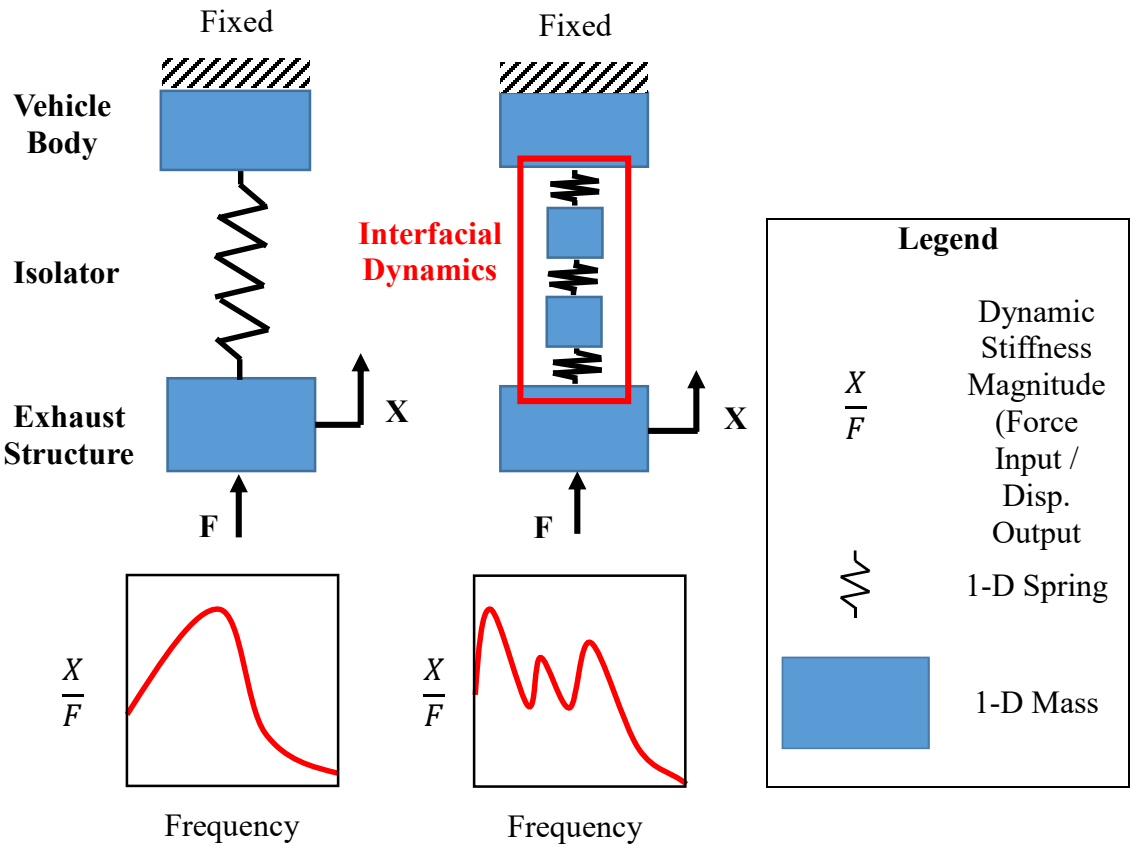

Figure 2: Illustrative Lumped System Representation

2 Problem Formulation

2.1 Problem Goal and Scope

The overall goal of this research is to better understand how the interfacial dynamics and multi-dimensional coupling of the isolator brackets affect the exhaust isolation system performance. Accordingly, the objectives are to (i) create a model with proper representation of the isolator bracket dynamics and exhaust structure, (ii) identify parameters for the model using modal experiments on components, (iii) design and use a bench experiment to validate the model for a given set of components, and (iv) exercise the model to quantify the effect of different isolator bracket designs and modifications to

component parameters (such as stiffness, damping, mass, etc.) on dynamic forces transmitted to the vehicle body in the 0 to 100 Hz frequency range.

For a tractable problem formulation using accepted frequency-domain modeling practices, the following assumptions are made. A flexible exhaust structure and isolator brackets with finite connection points are considered. Small harmonic forces and displacements are assumed. Linear elastic material properties and material loss factors are considered for the structures. The vehicle body and powertrain is assumed as rigid and massive in comparison to the exhaust structure, dictating conditions with no force or motion back-coupling from these bodies. The isolators are assumed to carry no moment, as such only translational terms for force and motion will be considered. Isolation performance is defined as vertical force transmitted to the vehicle body due to a vertical powertrain input force. An illustrative system model concept is shown in Figure 3.

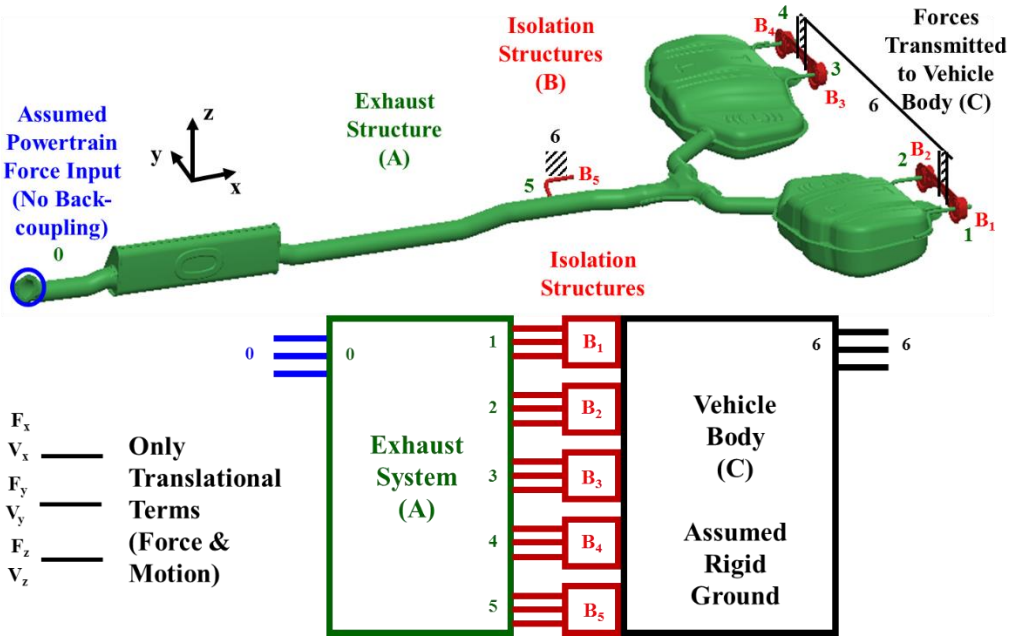

Figure 3: Illustrative System Model Concept

2.2 System Model Substructuring Convention

A system model substructuring convention is defined in Figure 4. There are two structures: the exhaust structure (A) and the isolation structures (B). On the exhaust structure, there is one input node (1), located at on a flange on the exhaust structure closest to the powertrain. At this node a three-dimensional force vector can be input. On the exhaust structure, there are five output nodes (2), each with their own three-dimensional velocity $\underline{V}$ and force $\underline{F}$ vectors, located at the exhaust hanger locations. The isolation structures (B) are composed of four isolator brackets and one middle hanger, comprising five connection nodes (2), each with three-dimensional velocity and force vectors. Each of the isolation structures are grounded at three-dimensional nodes (3). Accordingly, the model is assembled assuming that forces on substructure A at node group 2 ($\underline{F}_2^A$) are equal, but opposite, of the forces on substructure B at node group 2 ($\underline{F}_2^B$). Likewise, the velocities of node group 2 on substructure A ($\underline{V}_2^A$) are equal to the velocities on node group 2 on substructure B ($\underline{V}_2^B$).

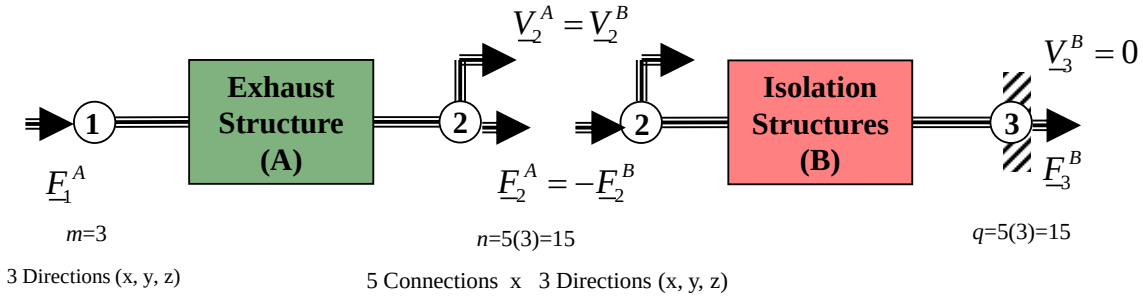

Figure 4: System Model Substructuring Convention

2.3 Exhaust Model Construction

In order to develop the substructure model for the exhaust structure, first a FEA model for the exhaust is created and a frequency analysis is run. Then, a modal experiment is performed on the physical exhaust structure to obtain the free-free mode shapes and natural frequencies. The FEA model is then tuned, by refining mesh dimensions, to match the modal experiment. The last step is to use the FEA model to calculate the exhaust structure mobility matrices.

2.3.1 Exhaust Structure FEA Model

The representative exhaust structure for this research is derived from that of the 2014 Buick LaCrosse sedan. The geometry is modeled using a solid modeling computer aided drawing (CAD) software. This CAD model is then imported into a FEA meshing software (HyperMesh [5]), and a primarily shell element mesh is generated, shown in Figure 5. Linear elastic steel material properties for the model are used, namely a Young's modulus of 207,000 MPa, a Poisson's ratio of 0.3, a density of 7.8×10^{-9} kg/mm^3, and structural damping of 0.001 (as reported in consistent units to be used by Abaqus CAE [6]). Because the piping for the exhaust has a thin thickness and the overall structure is relatively large, solid elements would require a very small element size, which would result in a computationally impractical model. For this reason, a shell element mesh is used for the piping, resonator, and mufflers. For the mounting rods, solid elements are used because not many elements are required to well define them due to the mounting rod's small size. By the same logic, some internal parts of the resonator are modeled using solid elements. Linear triangular elements are used for the mufflers due to coupling DOF errors to the mid-nodes of quadratic triangular elements when using

a tie constraint to the hanger mounting rods. A summary of the FEA model details, including color coding to Figure 5 for element types, is provided in Table 1.

Figure 5: Exhaust Structure FEA Model

Table 1: Exhaust Structure FEA Model Details

Mufflers (Blue)	Linear Triangular Shell Elements (S3)
Pipe and Resonator (Red)	Quadratic Triangular Shell Element (STRI65)
Mounting Rods (Green)	Quadratic Tetrahedral Solid Elements (C3D10M)
Number of Elements	61,800
Boundary Condition	Free-Free
Model Units	N, kg, mm, MPa

2.3.2 Exhaust Structure Free-Free Modal Experiment

Ten tri-axial accelerometers (PCB356A15) are arranged on the exhaust structure as shown in Figure 6, and an impulse input is applied to the driver side tail pipe using a modal impact hammer (PCB086B03). Bungee cords are used on the mounting rods at the muffler end to simulate a free-free boundary condition. Frequency response functions are obtained in LMS Test.Lab [7] data acquisition software with a frequency range of 512 Hz and a frequency resolution of 1 Hz. The PolyMax tool [7] is used to extract the modal parameters of the model (natural frequencies, mode shapes, and damping ratios) between 0-100 Hz. The locations of the accelerometers on the exhaust structures are mapped in a

geometric space in the software such that the mode shapes could be visually identified and matched qualitatively to free-free modes obtained through FEA.

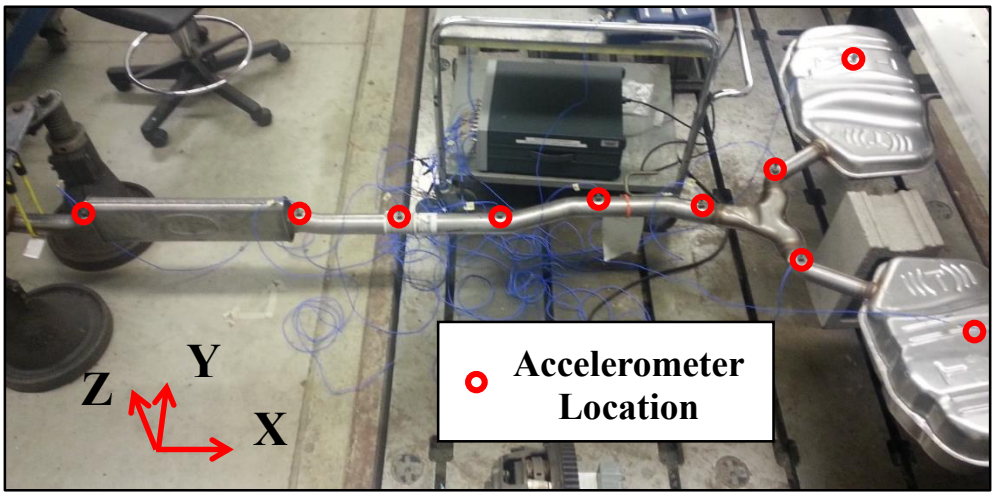

Figure 6: Exhaust Modal Experiment Setup

2.3.3 Exhaust Model Correlation and Model Improvement

The first seven mode shapes and the corresponding natural frequencies for the exhaust structure are matched qualitatively between the exhaust structure FEA frequency analysis (completed in Abaqus CAE [6]) and the experimental modal testing. In order to achieve a reasonable agreement of around 1-3 Hz between the exhaust structure FEA model and the experimental testing for each mode shape, various model improvements are made. From the initial model, many areas of the mesh where the software had failed to properly fit elements to the geometry are removed and manually meshed. Some parts of the original geometry contain gaps, requiring manual meshing to close the gap or the use of a tie constraint. In addition, local mesh size refinement is systematically applied to the mesh in order to achieve the desired improvement in model agreement while still maintaining a balance in model size for computational times. A final improvement is

made by manually adjusting the position of nodes for the elements in order to clean up some of the poor quality elements in the model due to factors such as element aspect ratio. A comparison between the free-free natural frequencies from the tuned FEA model and experiment is given in Table 2 for each matched mode shape. The first seven mode shapes from the FEA analysis are given in Figure 7 and are color coded with the corresponding natural frequency in Table 2. By refining the model through the removal of the gaps and the adjustment of the weld connection thickness, the desired agreement in natural frequencies is able to be achieved.

Table 2: Free-Free Natural Frequencies

Mode	Tuned FEA: Freely Suspended Conditions	Experiment: Suspended from Bungee Cords
1	13	13
2	18	18
3	21	23
4	44	45
5	46	48
6	59	57
7	63	63

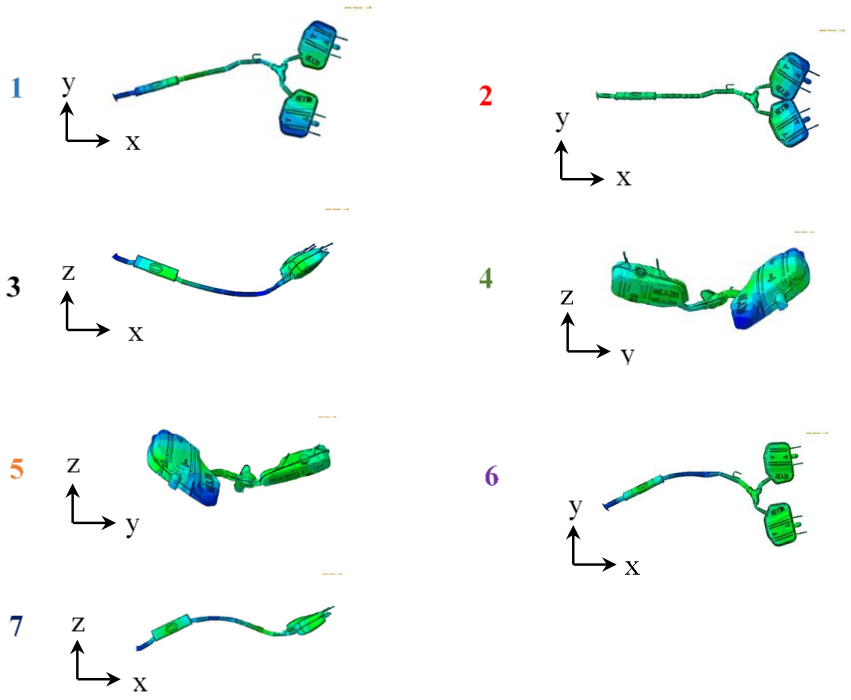

Figure 7: FEA Free-Free Mode Shapes

2.3.4 Exhaust Model Substructure

Connection nodes at the four bracket hanger structures, middle isolator hanger structure, and the powertrain end of the exhaust pipe, are defined on the tuned exhaust structure. Using FEA frequency analysis in Abaqus CAE [6], the first 50 eigenvalues and corresponding mass-normalized eigenvectors are extracted with each element at a connection node. Using MATLAB [4], the synthesized compliance frequency response function (FRF) matrix at a specific frequency ω_k in rad/s is calculated, given as

$$\tilde{\underline{\underline{H}}}^{A}(\omega_k) = \sum_{i=1}^{N} \frac{\underline{\phi}_i \underline{\phi}_i^T}{\left(\omega_{n,i}^2 - \omega_k^2\right) + \left(j2\zeta_i \omega_{n,i} \omega_k\right)} \qquad (1)$$

where N is the number of modes, $\underline{\phi_i}$ is the i^{th} mass normalized eigenvector, $\omega_{n,i}$ is the natural frequency in rad/s at the i^{th} mode, and $\zeta_{n,i}$ is the modal damping ratio at the i^{th} mode.

Using the synthesized FRF matrix in MATLAB [4], the exhaust structure mobility matrices at a specific frequency ω_k in rad/s are calculated as

$$\underline{\underline{\tilde{Y}}}^A(\omega_k) = j\omega_k \underline{\underline{\tilde{H}}}^A(\omega_k). \qquad (2)$$

These matrices are used later for the FRF-based substructuring system model, selected from $\underline{\underline{\tilde{Y}}}_A$ using the following conventions in the frequency domain:

$$\tilde{Y}_{22}^A = \left.\frac{\tilde{V}_2^A}{F_2^A}\right|_{F_1^A=0}, \qquad (3)$$

$$\tilde{Y}_{12}^A = \left.\frac{\tilde{V}_1^A}{F_2^A}\right|_{F_1^A=0}, \qquad (4)$$

and

$$\tilde{Y}_{21}^A = \left.\frac{\tilde{V}_2^A}{F_1^A}\right|_{F_2^A=0}. \qquad (5)$$

2.4 Isolator Bracket Model Construction

For the isolator bracket model, first a FEA model is created. This FEA model is then exercised to obtain various component parameters. These parameters are then input into a lumped parameter model. Experiments are performed on the isolator bracket and the results are used to improve the lumped parameter model.

2.4.1 Isolator Bracket FEA Model

A simplified geometry of the isolator bracket is created in CAD including only a single side of the isolator bracket. This simplification is made with the assumption that a

boundary condition along the cut side of the isolator bracket responds similarly to the isolator bracket fixed to the vehicle body. In addition, since the isolator bracket is symmetric, only one side needs to be simulated. Using this geometry, the FEA model is then meshed using solid elements. A reference point at the center of the isolator is created and kinematically coupled to the nodes on the inside surface of the isolator. Linear elastic isotropic material properties are considered. A static analysis is run by individually applying displacements in each direction to the reference point and measuring the reaction force. Similarly, a steady-state dynamic analysis is run by applying a harmonic displacement to the reference point and reading out the reaction forces. By taking the reaction forces and dividing them by the displacements first for the static analysis and then for the steady-state dynamic analysis, the respective static and dynamic stiffness parameters for the isolator bracket are obtained. In addition, a frequency analysis is run to get the natural frequencies for the constrained bracket assembly.

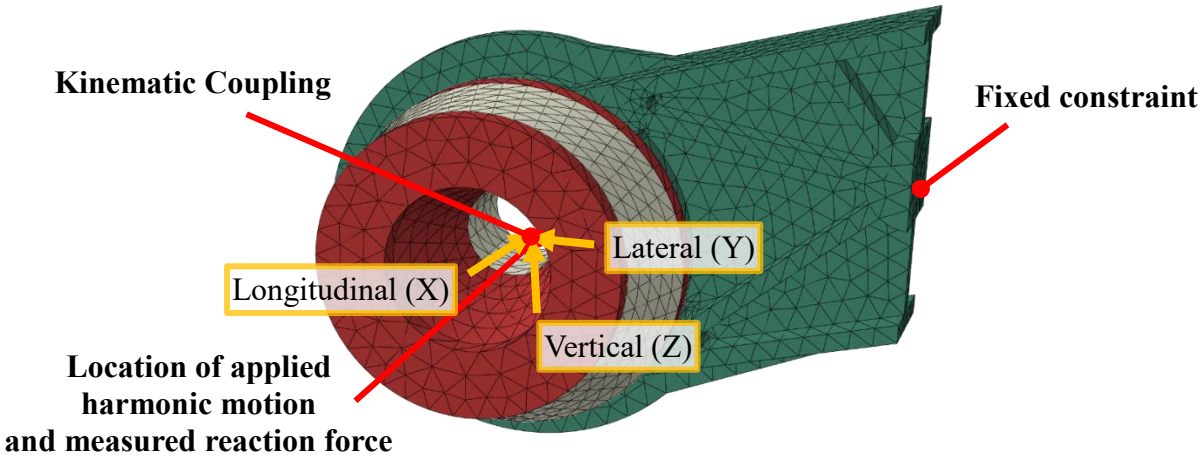

Figure 8: Isolator Bracket FEA Model

Table 3: Isolator Bracket FEA Model Material Properties

Material	Aluminum	Natural Rubber	Nylon
Young's Modulus [MPa]	69000	7	14500
Poisson's Ratio	0.33	0.45	0.35
Density [kg/mm^3]	2.7×10^{-9}	1.1×10^{-9}	1.6×10^{-9}
Loss Factors	0.001	0.1	0.01
Mesh Color	Green	White	Red

Table 4: Isolator Bracket FEA Model Details

Element Types	Quadratic Tetrahedral Solid Elements (C3D10)
Number of Elements	11,145
Boundary Condition (Disp. U and Rot. Disp. U_R)	U_1-U_3=0,U_{R1}-U_{R3}=0
Model Units	N, kg, mm, MPa

2.4.2 Isolator Bracket Lumped Parameter Model

A lumped parameter model with two mass elements coupled by a three-dimensional stiffness matrix and then coupled to ground by another a three-dimensional stiffness matrix is created to represent the parameterized isolator bracket. Using the FEA model for the constrained isolator bracket assembly, the previously computed static stiffness parameters in each direction are input into the isolator bracket stiffness matrices. The effective mass terms, loss factors, and coupling stiffness terms (XY and XZ) are estimated by comparing the dynamic response of the lumped parameter model to the dynamic response of the FEA model. The parameters used are summarized in Table 5.

Table 5: Isolator Bracket Lumped Parameter Properties

Rubber Isolator	X-direction Stiffness [N/mm]	K_{xx1}	251
	X-Y Coupling Stiffness [N/mm]	K_{xy1}	0
	X-Z Coupling Stiffness [N/mm]	K_{xz1}	17
	Y-direction Stiffness [N/mm]	K_{yy1}	39
	Z-direction Stiffness [N/mm]	K_{zz1}	39
	Effective Mass [kg]	m_1	0.012
	Loss Factor	η_1	0.1
Bracket	X-direction Stiffness [N/mm]	K_{xx2}	3041
	Y-direction Stiffness [N/mm]	K_{yy2}	243751
	Z-direction Stiffness [N/mm]	K_{zz2}	36275
	Effective Mass [kg]	m_2	0.19
	Loss Factor	η_2	0.001

The resulting mass and complex stiffness matrices for the isolator bracket, assuming a displacement amplitude vector of $Q = \{x_1 \quad y_1 \quad z_1 \quad x_2 \quad y_2 \quad z_2\}^T$ of a harmonic function are given, respectively, as

$$\underline{\underline{M}} = \begin{bmatrix} m_1 & 0 & 0 & 0 & 0 & 0 \\ 0 & m_1 & 0 & 0 & 0 & 0 \\ 0 & 0 & m_1 & 0 & 0 & 0 \\ 0 & 0 & 0 & m_2 & 0 & 0 \\ 0 & 0 & 0 & 0 & m_2 & 0 \\ 0 & 0 & 0 & 0 & 0 & m_2 \end{bmatrix} \tag{6}$$

and

$$\underline{\underline{\tilde{K}}} = \begin{bmatrix} K_{xx1}(1+j\eta_1) & -K_{xy1}(1+j\eta_1) & -K_{xz1}(1+j\eta_1) & 0 & 0 & 0 \\ -K_{xy1}(1+j\eta_1) & K_{yy1}(1+j\eta_1) & 0 & 0 & 0 & 0 \\ -K_{xz1}(1+j\eta_1) & 0 & K_{zz1}(1+j\eta_1) & 0 & 0 & 0 \\ 0 & 0 & 0 & K_{xx2}(1+j\eta_2) & 0 & 0 \\ 0 & 0 & 0 & 0 & K_{yy2}(1+j\eta_2) & 0 \\ 0 & 0 & 0 & 0 & 0 & K_{zz}(1+j\eta_2) \end{bmatrix}, \tag{7}$$

where the subscript 1 indicates the isolator and subscript 2 indicates the bracket.

The driving point mobility matrices *Y* at a specific frequency ω_k are populated for each of these models by applying a unit force at the input of the isolator mass m_1 and

calculating the resulting velocity of the isolator mass m_1. The force transmissibility matrices T at a specific frequency ω_k are populated for each of these models by applying a unit force at the input of the isolator mass m_1 and calculating the resulting displacement of the bracket mass m_2 and multiplying each displacement term by the associated bracket stiffness term. These matrices are assembled for the isolation structure matrices using the following conventions in the frequency domain:

$$\tilde{Y}_{22}^{B} = \left. \frac{\tilde{V}_2^B}{F_2^B} \right|_{V_3^B=0} \tag{8}$$

and

$$\tilde{T}_{32}^{B} = \left. \frac{\tilde{F}_3^B}{F_2^B} \right|_{V_3^B=0} \tag{9}$$

and are used later for the FRF-based substructuring system model.

2.4.3 Isolator Bracket Lumped Parameter Model Tuning

Since actual material properties of natural rubber are not available for the model, two bench experiments are created to provide a means to tune the model. First, the assembly is secured in a vise on a bench setup. A known mass is applied to a bolt through the isolator and the resulting vertical deflection is measured using a height gage. From this experiment, the vertical static stiffness for the isolator is estimated and the material properties in the FEA model, specific Young's modulus of the rubber isolator, are modified (within acceptable range for natural rubber) to achieve this static stiffness.

Next, the isolator bracket assembly is fixed to the bench in a vise and an impact hammer (PCB 086B03) is used to apply a force input to the isolator insert in the longitudinal direction. One uni-axial accelerometer (PCB UJ352C66) is attached to the

isolator insert oriented in the longitudinal direction to sense the response from the force input. The resonant frequencies of the constrained isolator are identified from the measured FRF and compared to the results of a frequency analysis using the FEA model of the constrained isolator bracket. The material properties in the FEA model, specifically density, are modified (within acceptable range for natural rubber) to produce natural frequencies that match the experiment.

In a similar fashion, the lumped parameter model is tuned to match the natural frequencies and dynamic stiffness of the FEA model. This tuning is done by adjusting the mass terms and assumed loss factors. The dynamic stiffness for the tuned isolator bracket lumped parameter model compared to that for the FEA model are shown in Figure 9.

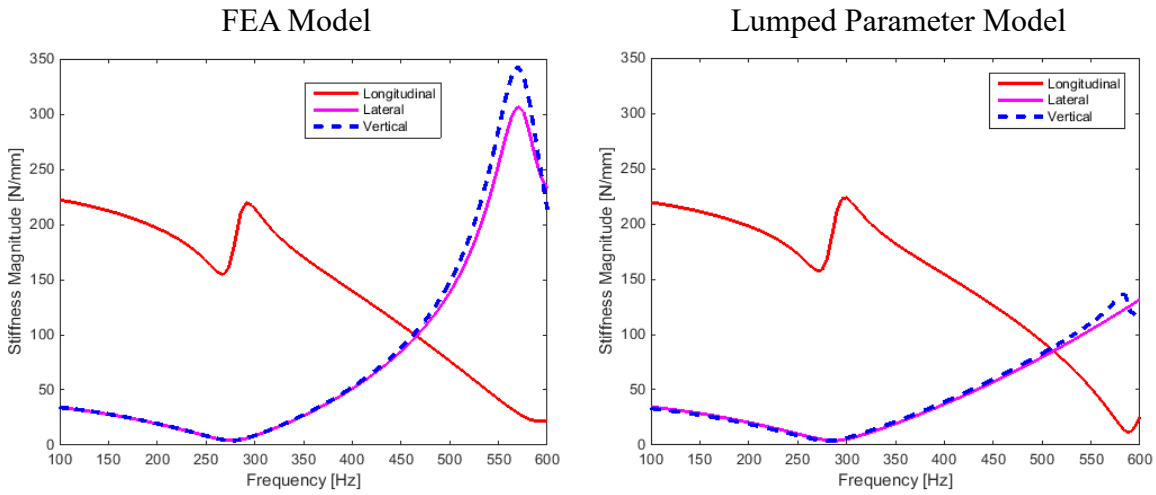

Figure 9: FEA Model Correlation to Lumped Parameter Model for Dynamic Stiffness Magnitude

Observing Figure 9, the longitudinal stiffness can be seen to match within 5 N/mm between the two models. However, the vertical and lateral stiffness vary in magnitude, particularly in the region above 450 Hz in which the FEA model is

substantially higher in magnitude. Staying in the 100-400 Hz region, the difference in dynamic stiffness for both models is within 5 N/mm.

2.5 Synthesized System Model and Validation

With each of the component substructures completed, the individual substructures are combined (synthesized) into a system level model. This procedure is done through a frequency-response-function-based substructuring method. Given a force vector on the exhaust structure at node 1 ($\underline{F}_1^A$), the force vector at a specific frequency ω_k on the isolation structures at node group 2 is given by

$$\underline{\tilde{F}}_2^B(\omega_k) = \left[\underline{\underline{\tilde{Y}}}_{22}^A(\omega_k) + \underline{\underline{\tilde{Y}}}_{22}^B(\omega_k)\right]^{-1} \underline{\underline{\tilde{Y}}}_{21}^A(\omega_k)\,\underline{F}_1^A(\omega_k). \tag{10}$$

The force vector transmitted to vehicle body through the isolation structures at a specific frequency ω_k is given by

$$\underline{\tilde{F}}_3^B(\omega_k) = \underline{\underline{\tilde{T}}}_{32}^B(\omega_k)\,\underline{\tilde{F}}_2^B(\omega_k). \tag{11}$$

The driving point accelerance of the exhaust structure at node 1 is easily measured in an experiment for model validation and can be calculated in the model by

$$\underline{\tilde{A}}_1^A(\omega_k) = j\omega_k\left[\underline{\underline{\tilde{Y}}}_{11}^A(\omega_k)\,\tilde{F}_1^A - \underline{\underline{\tilde{Y}}}_{12}^A(\omega_k)\,\underline{\tilde{F}}_2^B\right] \tag{12}$$

at a specific frequency ω_k.

In order to validate the model, a driving point modal impact experiment is performed at the powertrain end of the exhaust structure. On the physical structure, a uni-axial accelerometer (PCB UJ352C66) is placed near the location associated with node 1 of the exhaust structure in the model and oriented in the vertical (Z) direction. A modal impact hammer (PCB 086B03) is applied to the physical exhaust structure directly beside the accelerometer in the same sensing direction. The accelerance FRF is measured

using a National Instruments CompactDAQ Data Acquisition with NI9234 module. A picture of the location of the input location and the accelerometer location is shown in Figure 10.

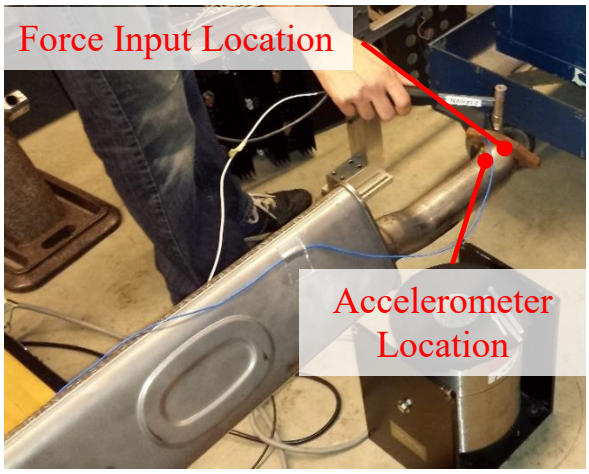

Figure 10: Modal Impulse Hammer Experiment

The synthesized model is then run and the accelerance at the powertrain end of the exhaust is calculated. The accelerance data from the experiment is imported and plotted with the accelerance calculated from the synthesized model. The results for the simulation and experiment are shown in Figure 11.

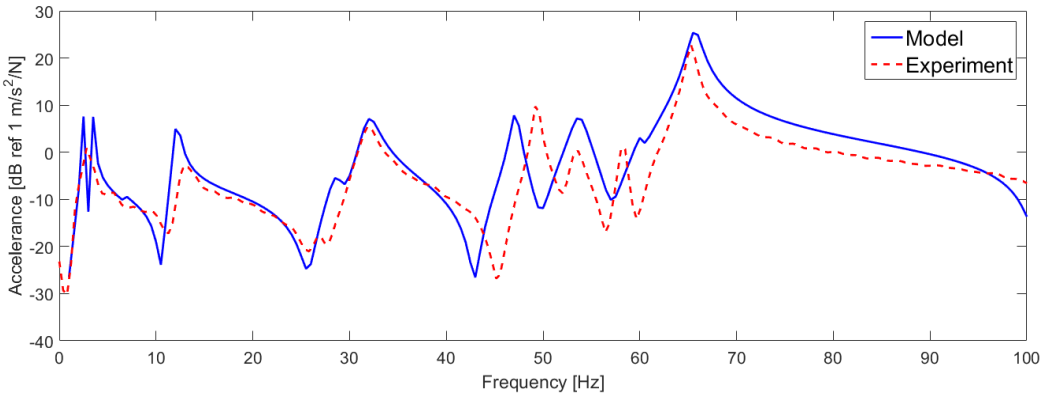

Figure 11: Synthesized Model Accelerance Correlation to Experiment

When examining the results, it can be seen that many peaks coincide, while others are shifted by only 1-2 Hz. Also, most resonances and anti-resonances share similar magnitude. Looking at plot, the model and experiment match relatively closely up until about 45 Hz. Around 12 Hz, the model is about 5 dB above and below the experimental resonance and anti-resonance respectively, however both shapes match closely. At about 27 Hz, we can see that the smaller resonance is shifted to the right on the model, but by less than 2 Hz. Due to the close proximity of the larger resonance at 33 Hz, this small shift of the smaller resonance results in a large disparity of around 10 dB between the model and experiment accelerance values at those frequencies.

At 45-50 Hz, the model experiences a shift to the left of a little over 2 Hz relative to the experiment for the resonance and anti-resonance, however the magnitude for model and experiment are similar. At about 55 Hz, the frequency for the resonance matches up closely between the model and experiment, however the model has a magnitude of about 6 dB higher. Around 58 Hz the model is shifted under 2 Hz to the right with a difference in magnitude of less than 2 dB. Finally, we see the model match the shape for 65 Hz and above, however the magnitude is often 3 dB higher than the experiment, except at 95-100 Hz where it dips below.

3 Results

With the synthesized model created in MATLAB [4], parametric studies are conducted by systematically modifying parameters in the lumped parameter isolator component model within the synthesis model in order to determine the influence of each parameter with respect to exhaust isolation system performance. The exhaust isolation system performance is defined as the total vertical force transmitted for 1 N vertical

powertrain force over the 1-100 Hz range. This is calculated by applying an input force vector $\underline{F}_1^A = \{0 \quad 0 \quad 1\}^T$ to the exhaust structure at node 1 and summing the vertical components related to the isolator brackets of the transmitted force vector $\underline{\tilde{F}}_3^B$ from Equation 11. The first study is primarily concentrating on the effect of mass for each of the components. The second study is investigating component damping. The final study is looking at the isolator longitudinal stiffness and coupling.

3.1 Case I: Effect of Isolator and Bracket Mass

The first case study is run to examine the effect of the isolator and bracket mass. The isolator mass is increased in the synthesis model from a baseline of 0.12 kg to 0.36 kg, representing a change of nylon insert material to aluminum. The system responses for the baseline isolator mass, as well as the increased isolator mass, are calculated and plotted in MATLAB [4] and are shown in Figure 12.

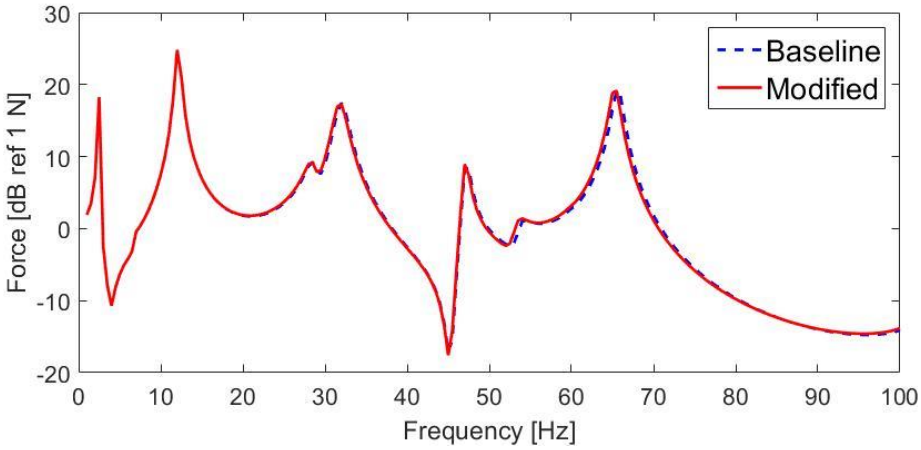

Figure 12: Effect of Isolator Mass on Total Vertical Transmitted Force Through the Isolator Brackets

Looking at the effect on the system response, it is shown that an increase in isolator mass has no perceivable effect at frequencies below 20 Hz. For most of the 20-100 Hz range, a very small increase of less than 0.5 dB in force transmitted is observed.

In a similar fashion, in order to examine the effect of the bracket mass, the baseline case for bracket mass of 0.19 kg is increased in the model to 1.33 kg. The responses for both are plotted in Figure 13.

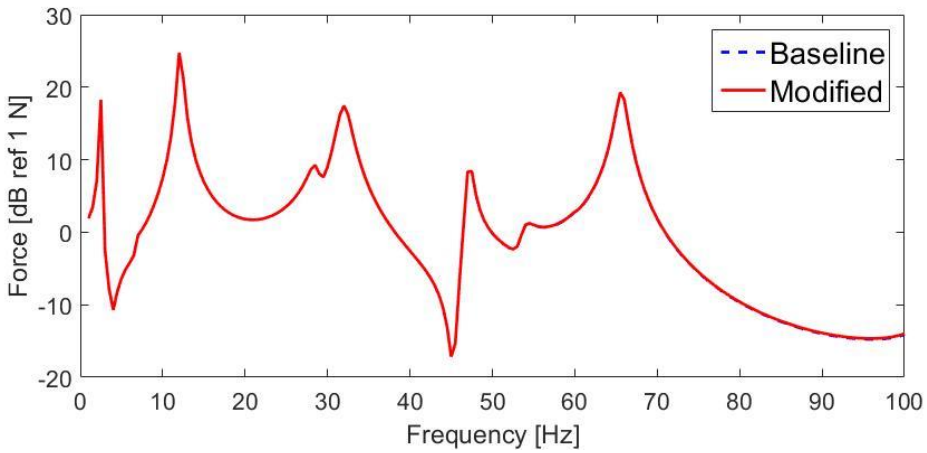

Figure 13: Effect of Bracket Mass on Total Vertical Transmitted Force Through the Isolator Brackets

When the forces transmitted are calculated for both of these cases, no differences are observed below 55 Hz. In the 55-100 Hz range, a nominal increase of less than 0.5 dB can be detected around 60 Hz and above 75 Hz.

3.2 Case II: Effect of Isolator and Bracket Damping

A second case is run in order to look at the effect of component damping on the forces transmitted. For the isolator, the loss factor is increased from the original value of 0.1 to a value of 0.5, representing a change to a fluid or grease filled isolator. The results for the isolator are shown in Figure 14.

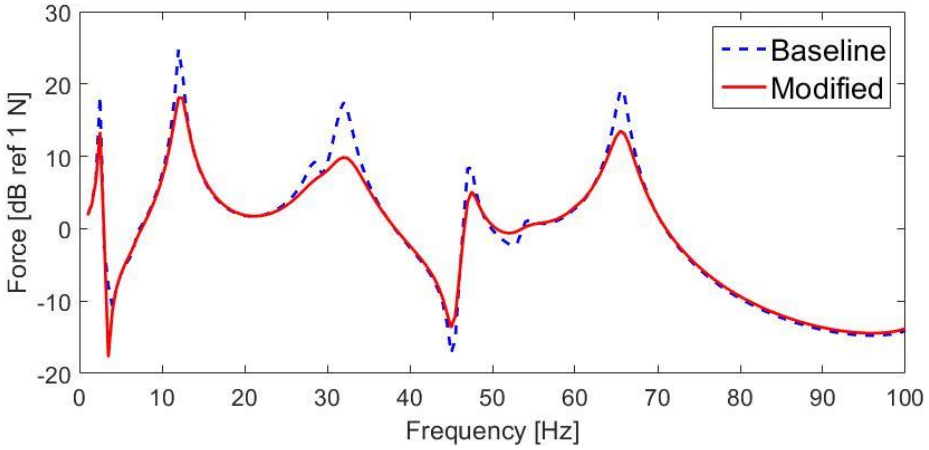

Figure 14: Effect of Isolator Damping on Total Vertical Transmitted Force Through the Isolator Brackets

From the model, it is shown that increasing the isolator damping has a substantial impact on the forces transmitted throughout the frequency range of interest. At almost every frequency, the additional damping from increase in loss factor provides large attenuation, especially at peaks. At some peaks, the decrease is as much as 5 dB. The exception to this attenuation occurs at two troughs around 45 Hz and 55 Hz where there is an amplification of around 3 dB. In addition, above 75 Hz the additional damping results in a very small increase of less than 0.5 dB in forces transmitted.

To investigate damping for the bracket, the baseline value of 0.001 is increased to 0.1, representing a constrained layer damping modification to the bracket structure. When the responses are calculated in the synthesized model, no difference is found.

3.3 Case III: Effect of Isolator Coupling and Longitudinal Stiffness

For the final case, both the isolator coupling and longitudinal stiffness factors are investigated to determine the influence on the system with respect to forces transmitted. For the isolator coupling, the stiffness coupling terms in the X and Z directions (k_{xz1}) in

the isolator lumped parameter model are set to zero and compared to the baseline. The results for the removal of the isolator coupling are shown in Figure 15.

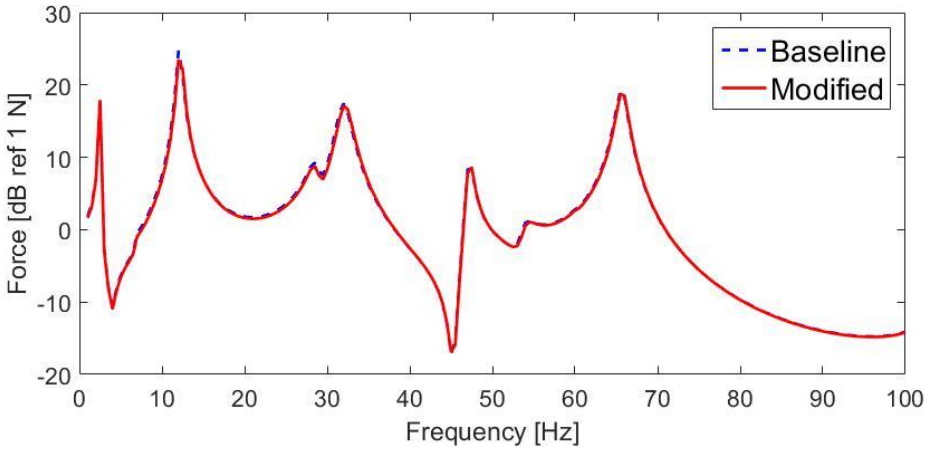

Figure 15: Effect of Isolator Coupling on Total Vertical Transmitted Force Through the Isolator Brackets

From the results, removing the coupling terms results in a very small decrease in force transmitted across the frequency range of interest. In most cases, there is less than 0.5 dB decrease, except for at about 15 Hz where there is around 1 dB attenuation.

The next subject of testing is that of the inline isolator stiffness (k_{xx}) in the longitudinal direction. From the baseline design, the inline longitudinal stiffness is increased from a value 10 N/mm to 200 N/mm. The result is shown in Figure 16.

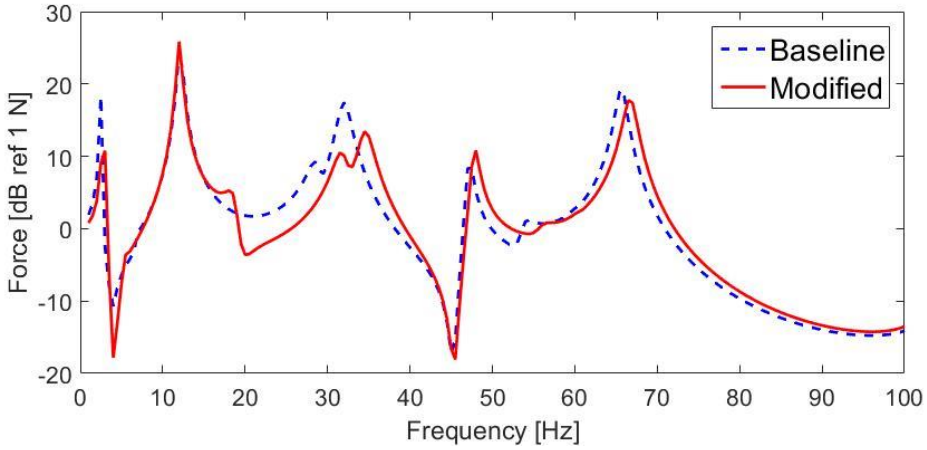

Figure 16: Effect of Isolator Longitudinal Stiffness on Total Vertical Transmitted Force Through the Isolator Brackets

When looking at the results, the impact of the longitudinal stiffness on the system response can be seen to be considerable. From around 20-40 Hz, the response is shifted to the right around 3 Hz in addition to experiencing some attenuation, in some points as much as 5 dB. In the 0-10 Hz, there is a large decrease at the peak and troughs of about 7 dB. Above 45 Hz, the response is shifted about 1 Hz to the right resulting in nominal increases and decreases of less than 0.5 dB.

The final subcase reviewed examines the influence of the isolator coupling terms on an initial design that maintains the higher isolator inline longitudinal stiffness (k_{xx}) from the previous subcase. In this simulation, the baseline has an inline isolator longitudinal stiffness of 200 N/mm and includes the XZ coupling terms (k_{xz1}). The modified model retains this increased longitudinal stiffness while removing the XZ coupling terms. The results are shown in Figure 17.

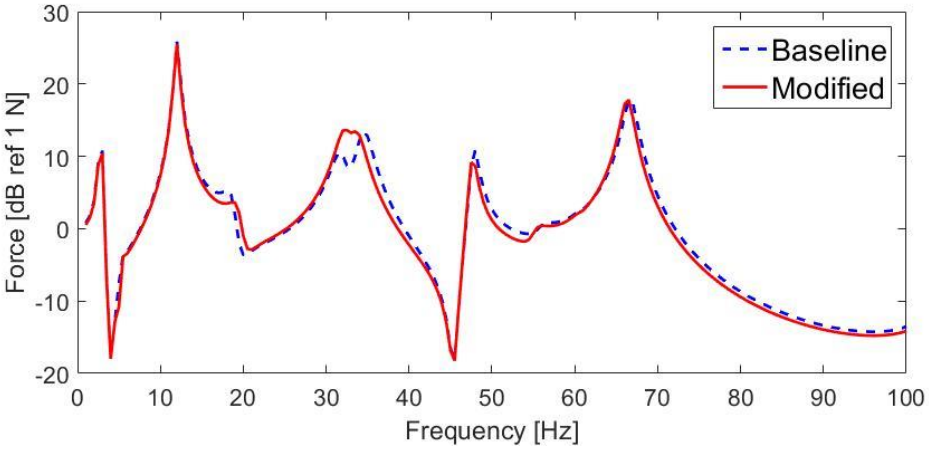

Figure 17: Effect of Coupling with Baseline Higher Isolator Longitudinal Stiffness on Total Vertical Transmitted Force Through the Isolator Brackets

The effect of removing the coupling terms for a higher isolator longitudinal stiffness proves to be considerable. By removing the coupling terms, the peak previously at about 32 Hz is shifted to the right, resulting in an amplification of around 3 dB. However, at the other peaks, there tends to be a small decrease between 0.5-1 dB.

4 Conclusions

4.1 Summary

A parameterized model-based system model with proper representation of the exhaust structure and isolator bracket is created to investigate the effect of interfacial dynamics and multidimensional coupling on exhaust isolation performance. Exhaust isolation performance is defined as the vertical transmitted force per force input through exhaust structure into the vehicle body. The changed parameters for each design study, as well as the amount changed and approximate effect on the force transmitted to the vehicle body, are summarized in

Table 6 below.

Table 6: Summary of Sensitive Parameters

Parameter	Amount Changed	Force Transmitted (< 0.5 dB Nominal)
Isolator Mass	3x increase	Nominal
Bracket Mass	7x increase	Nominal
Isolator Loss Factor	5x increase	- 5 dB
Bracket Loss Factor	100x increase	Nominal
Coupling	Removing Coupling	- 1 dB
Longitudinal Stiffness	20x increase	+/- 5 dB
Longitudinal Stiffness and Coupling	Removing Coupling	+/- 3 dB

When reviewing the summary of the results, it can be observed that even a large change in stiffness parameters for the bracket yields a nominal difference in force transmitted. This conclusion makes sense as it is relatively stiff and not cantilevered far from the vehicle body fixture. If it is stiff and the free end is relatively short, the bracket is not as likely to participate in the vibration; therefore, its mass and damping have little effect on the exhaust isolation system performance.

In addition, the results show that inclusion of the isolator bracket interfacial dynamics, specifically the inclusion of the interfacial masses, have minimal influence on isolation performance. The effect of the interfacial dynamics will likely be more pronounced at frequencies outside of those considered in this study, specifically closer to the isolator bracket resonances and the local hanger modes (observed in the FEA of the exhaust structure above 100 Hz). The effect of including coupling on isolation

performance shows some impact, typically increasing the force transmitted. However, when the isolator longitudinal stiffness in increased, the effect of coupling is considerably more pronounced.

4.2 Future Work

This model has the potential to be improved in a number of ways. One such method would be the inclusion of rotational coupling in the model to determine whether its effect is impactful, as right now only translational terms for force and velocity are considered. Another step that could be taken is to model the vehicle body structural dynamics and incorporate them into the model in order to ensure that the assumption of the vehicle body as ground is not an oversimplification. This model could also be extended to different exhaust isolation designs to evaluate its robustness, such as different exhaust structures with various hanger mounting points as well as different isolator bracket geometries. Further studies could be put into investigating the interaction of the exhaust structure with respect to the vehicle powertrain and suspension in order to improve modeling accuracy. The boundary conditions imposed on the isolator bracket assuming it is perfectly fixed to the vehicle body in the center could be examined by extending the bracket FEA model to include the entire bracket as well as modeling the bolted connections imposed on the bracket. One final extension could be a full vehicle test with realistic road inputs.

4.3 Applications

These studies provide insight into the influence of the interfacial dynamics of the isolator brackets and their interaction with the exhaust structure. The modeling procedure proposed has potential to be used early in the vehicle design process to identify

improvements to a baseline design. The synthesis procedure proposed provides a means to quickly modify the isolation connection dynamics without continually running computationally intensive FEA models of the entire system. Likewise, the synthesis methods can also be used to identify targets for component performance and potential weight reduction by quickly interrogating the design space. With a more efficient design process, fewer intermediate prototypes will also need to be created, potentially reducing design cycles and development costs.

References

[1] Chen, X., Y. Zhang, Y. Zhang, and M. Jiang, “Hanger Location Design and Vibration Isolation of an Exhaust System,” *SAE Technical Paper,* 2014-01-1708, 2014.

[2] Galindo, M., “Mobility at the Development of Exhaust System,” *SAE Int. Journal of Passenger Cars – Mechanical Systems,* 4(2), 983-988, 2011.

[3] Hamada, M., “Development of High Performance Exhaust Mountings,” *SAE Technical Paper,* 940613, 1994.

[4] *MATLAB 2015b*. Computer software. Mathworks, Inc., 2016. Retrieved from <http://www.mathworks.com/products/matlab/>

[5] *HyperMesh 13.0*. Computer software. Altair Engineering, Inc., 2016. Retrieved from < http://www.altairhyperworks.com/product/HyperMesh>

[6] *Abaqus/CAE 6.13*. Computer software. Dassault Systèmes Simulia Corp., 2016. Retrieved from <http://www.3ds.com/products-services/simulia/products/abaqus/abaquscae/>

[7] *LMS Test.Lab 14*. Computer software. Siemens Product Lifecycle Management Software Inc., 2016. Retrieved from < http://www.plm.automation.siemens.com/en_us/products/lms/testing/test-lab/>

List of Symbols

$\underline{\underline{\tilde{A}}}$	accelerance matrix
$\underline{\underline{\tilde{H}}}$	synthesized FRF matrix
j	$\sqrt{-1}$
$\underline{\underline{K}}$	stiffness matrix
$\underline{\underline{M}}$	mass matrix
$\underline{\underline{\tilde{T}}}$	force transmissibility matrix
$\underline{\underline{\tilde{Y}}}$	mobility matrix
ξ	modal damping ratio
$\underline{\phi}$	mass normalized mode shape
ω	frequency [rad/s]

Subscripts

i	i^{th} mode
k	index
mp	from node p to node m
n	natural
q	located at node q
_	vector
_	matrix

Superscripts

A	exhaust substructure
B	isolator bracket substructure
T	transposed matrix
-1	inverse
~	complex value